

An evolutionary approach to real-time moment magnitude estimation via inversion of displacement spectra

M. Caprio,¹ M. Lancieri,² G. B. Cua,¹ A. Zollo,³ and S. Wiemer¹

Received 6 September 2010; revised 10 November 2010; accepted 24 November 2010; published 20 January 2011.

[1] We present an evolutionary approach for magnitude estimation for earthquake early warning based on real-time inversion of displacement spectra. The Spectrum Inversion (SI) method estimates magnitude and its uncertainty by inferring the shape of the entire displacement spectral curve based on the part of the spectra constrained by available data. The method consists of two components: 1) estimating seismic moment by finding the low frequency plateau Ω_0 , the corner frequency f_c and attenuation factor (Q) that best fit the observed displacement spectra assuming a Brune ω^2 model, and 2) estimating magnitude and its uncertainty based on the estimate of seismic moment. A novel characteristic of this method is that it does not rely on empirically derived relationships, but rather involves direct estimation of quantities related to the moment magnitude. SI magnitude and uncertainty estimates are updated each second following the initial P detection. We tested the SI approach on broadband and strong motion waveforms data from 158 Southern California events, and 25 Japanese events for a combined magnitude range of $3 \leq M \leq 7$. Based on the performance evaluated on this dataset, the SI approach can potentially provide stable estimates of magnitude within 10 seconds from the initial earthquake detection. **Citation:** Caprio, M., M. Lancieri, G. B. Cua, A. Zollo, and S. Wiemer (2011), An evolutionary approach to real-time moment magnitude estimation via inversion of displacement spectra, *Geophys. Res. Lett.*, 38, L02301, doi:10.1029/2010GL045403.

1. Introduction

[2] Earthquake early warning (EEW) attempts to provide subscribers seconds to tens of seconds of warning before the onset of damaging ground shaking. EEW systems are currently operational and providing warning information in Japan, Mexico, Romania, Taiwan, and Turkey, while methodologies are being developed and tested throughout the United States, Europe, and Asia. We refer the reader to the work by *Allen et al.* [2009] for an up-to-date summary of EEW efforts around the world.

[3] Several evolutionary magnitude estimation methods are described in the literature and are currently under testing or development in seismic networks around the world. The

ElarmS [*Allen and Kanamori, 2003*] and Virtual Seismologist [*Cua et al., 2009*] algorithms are network-based EEW approaches that apply evolutionary magnitude estimation approaches and are being tested in real-time in California as part of the California Integrated Seismic Network EEW project. These methods relate measures of predominant period (τ_p), in the case of ElarmS, or ground motion ratios, in the case of Virtual Seismologist, to magnitude via empirical relationships. The RTMag (Real-Time Magnitude estimation) approach [*Lancieri and Zollo, 2008*], which estimates magnitude from measures of peak displacement (PD), is being tested as part of the PRESTo [*Satriano et al., 2010*] real-time system being tested at the ISnet (Irpinian Seismic network) network in Southern Italy. Methods such as these can be considered predictive relationships. These predictive relationships involve scaling quantities measured from the initial portions of the P-wave (i.e., predominant period, ground motion ratios, low-pass filtered displacement) that are not part of standard, non-real-time magnitude calculations, with the final magnitude. The main advantage of these predictive relationships is that the final magnitude can be estimated with only few seconds of waveform data, potentially increasing the available warning time. On the other hand, their validity on a wide magnitude range is object of debate in the scientific community.

[4] In contrast, the EEW systems implemented in Japan [*Kamigaichi et al., 2009*] and in Mexico [*Espinosa-Aranda et al., 2000*] employ empirical (as opposed to predictive) relationships. These systems use quantities that are part of standard, non-real-time magnitude estimation (maximum displacement amplitude in the case of Mexico, and a combination of energy and growth rate measures, in the case of Japan), but evaluate these parameters on the available waveform data (starting with few seconds of P-wave) to provide evolutionary magnitude estimates. These empirical methods naturally underestimate the final magnitude in the first seconds, but approach reliable magnitude estimates as additional data become available. The advantages of these empirical methods are that 1) they do not rely on correlations between quantities measured in the first few seconds and the final event magnitude, and 2) they are valid over a broad magnitude range.

[5] In Japan, the system takes advantage of the high station density (average station spacing of 20 km [*Kamigaichi et al., 2009*]). The Mexico system benefits from the large distance between the source zone along the Guerrero coast and their target warning areas of Mexico City and Oaxaca, at ~ 320 and ~ 150 km away, respectively.

[6] In this study we develop the Spectral Inversion (SI) method for regional EEW magnitude estimation. The SI approach is based on real-time, evolutionary computation of

¹Swiss Seismological Service, ETH Zurich, Zurich, Switzerland.

²École Normale Supérieure, Paris, France.

³Scienze Fisiche, Università Federico II di Napoli, Naples, Italy.

the displacement spectrum and direct estimation of the seismic moment and moment magnitude.

2. The Spectrum Inversion Method

2.1. Spectral Model

[7] Following *Abercrombie* [1995], we use the following expression to model the displacement spectra of P and S waves:

$$\Omega(f) = \frac{\Omega_0}{\sqrt{\left[1 + \left(\frac{f}{f_c}\right)^\gamma\right]^{\frac{n}{2}}}} \exp^{-\frac{t}{Q}} \quad (1)$$

where $\Omega(f)$ is the Fourier amplitude of the P- or S-wave displacement, Ω_0 is the low frequency plateau, f_c is corner frequency, n the high-frequency fall off rate on a log-log plot, and γ is a constant. If $n = 2$, and $\gamma = 1$, equation (1) is the spectral shape proposed by *Brune* [1970]. Similar to *Abercrombie* [1995], we fix $\gamma = 2$. This modification produces a sharper corner than *Brune's* [1970] original model. The exponential term expresses the anelastic attenuation, with Q as the frequency-independent quality factor and t the travel time of the considered wave.

[8] We relate Ω_0 to seismic moment using *Aki and Richards's* [2002] relation

$$M_0 = \frac{4\pi\rho_r^{1/2}\rho_s^{1/2}rc_r^{1/2}c_s^{5/2}\Omega_0}{R_cF_s} \quad (2)$$

where M_0 is seismic moment in (N/m), ρ_r is the density in (km/m³) at the receiver (or station), ρ_s is the density at the source, r is the hypocentral distance in (km), c_r the shear wave velocity at the station in (km/s), c_s the shear wave velocity at the source in (km/s), and Ω_0 is the value of the spectral plateau at low frequency. R_c (=0.63) and F_s (=2) are factors accounting for the average radiation pattern and free surface effects, respectively.

[9] Given the seismic moment estimated from equation (2), we then estimate moment magnitude using *Hanks and Kanamori's* [1979] relationship and via

$$\log M_0 = 1.5M_w + 9.05 \quad (3)$$

where M_w is moment magnitude and M_0 is seismic moment in N/m.

2.2. Inversion Process

[10] The SI method is intended as an evolutionary magnitude estimation approach for possible application in EEW. Required input parameters are real time location estimate and at least one second of record from the on-going event. In the description that follows, we assume that a location estimate is available from a separate algorithm.

[11] The SI approach involves: 1) calculating the displacement spectra for all available components at a given station, 2) simultaneously inverting for the low frequency plateau, the corner frequency, and Q for each available component, 3) estimating seismic moment using equation (2), and 4) estimating moment magnitude from seismic moment using equation (3). The three-parameter inversion for the plateau value, corner frequency, and Q is performed using the Nelder-Mead (1965) simplex algorithm. The

seismic moment at a given station is estimated using equation (2), with Ω_0 being the vector sum of the plateau values from the three components. The station-specific seismic moment estimates are then averaged to arrive at a seismic moment estimate for the event (and its uncertainty):

$$\bar{M}_0 = \frac{\sum_{i=1}^n M_{0,i}}{n} \quad \sigma_{M_0} = \sqrt{\frac{\sum_{i=1}^n (\bar{M}_0 - M_{0,i})^2}{n-1}} \quad (4)$$

where the i ranges over the n stations with at least one second of waveform data following the P-detection, $M_{0,i}$ is the seismic moment estimated at the i^{th} station and σ_{M_0} is the standard deviation.

[12] The SI magnitude estimates are updated each second. The evolution of the SI estimation process with the increased availability of data is illustrated in Figure 1b, using waveforms from the 2008 M6.9 Iwate-Miyagi earthquake in Japan. The spectral inversion (and hence the magnitude estimation) process stabilizes as more the P-waves propagate to more distant stations and as longer time series are available at the stations. At a given station, the magnitude estimate stabilizes when the entire P phase is available for estimation.

[13] Correctly distinguishing between P, S, and surface waves is crucial to the SI approach. In the SI approach, the assumed location estimate and the known station coordinates are used to estimate the S-arrival times at the various stations. The difference in the S- and P- arrival times (S-P time) is then the length of the P-wave time window.

[14] While the criteria used to determine the length of the P-wave time window is relatively simple, determining the S-wave time window is more complicated. If the S-wave window is too short, the seismic moment will be underestimated. On other hand if the S-wave window is too long, the signal will include contributions from surface waves, leading to an elevation of the plateau level and overestimation of the seismic moment and moment magnitude.

[15] To estimate the length of the S phase at each station, we follow the approach proposed by *Madariaga* [1976], which relates the corner frequency to the rupture size at the source. We thus use the corner frequency estimate f_c to define the length of the S phase at each station that we assumed to be $2/f_c$.

[16] We take anelastic attenuation into account by inverting for quality factor Q for each waveform used in the analysis.

3. Method Application

3.1. Data and Processing

[17] We applied the SI magnitude estimation methodology off-line on waveform datasets from Southern California and Japan. For each event analyzed, we assumed the location listed in the earthquake catalogue.

[18] We used 70 $M \geq 4.0$ events available from the SCECDC from 1 Jan 2006 through 31 December 2008 with magnitude and location listed in the ANSS (Advanced National Seismic System) catalogue. We also included events $3 \leq M \leq 4$ which had at least 3 stations within 60 km epicentral distance. In general, we limited our study to stations within 60 km epicentral distance, due to our interest in

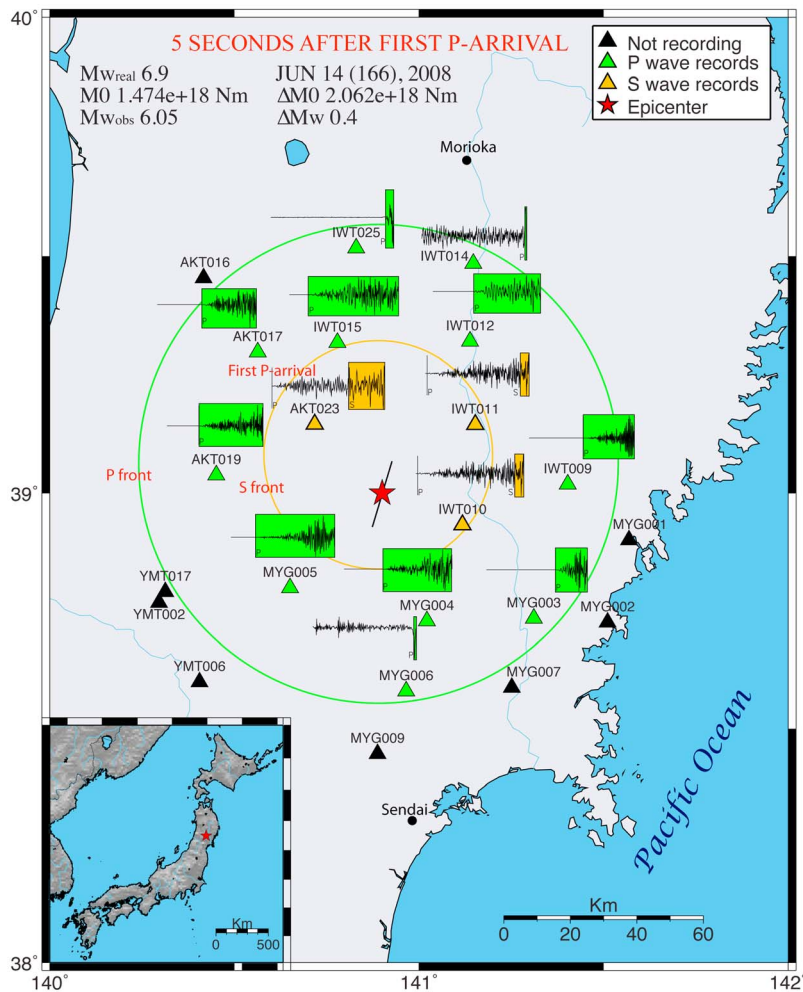


Figure 1a. The information available at the K-net and Kik-Net networks 5 seconds after the initial P-detection for the Iwate-Miyagi earthquake on 14 June 2008. In the figure the yellow and the green circles represent respectively the S- and the P-front after 5 seconds from the first detection.

EEW systems for target regions at short to intermediate distances from the earthquake source.

[19] We used 25 crustal events (depths $< 50\text{km}$) with $M \geq 5.8$ which occurred between 1996 and 2007. We used the magnitudes and locations listed in the manually revised F-Net catalogue. The joint Southern California - Japan waveform dataset spans the magnitude range $3 \leq M \leq 7$. Figure 2a shows the location of the test events relative to the network stations in Japan and California.

[20] We applied the SI method to the assembled waveform datasets. To simulate the data availability during real-time operation, we cut the waveforms at different stations using time windows of lengths t_n , where t_n is the difference between the current time and the P-pick arrival at the station. To illustrate this point, Figure 1a shows a snapshot of the available data at the various stations around the source region 5 seconds after the initial P-detection for the 14 June 2008 M7.0 Iwate-Miyagi in Japan.

[21] We used an automatic short-term average/long-term average (STA/LTA) picker [Allen, 1978] to determine the P arrival, T_p , at a given station. The S-arrival was determined based on the distance of the station to the event and an

average S-wave velocity (3.5 km/s). At each given time, T_n , we used the available broadband or strong motion time series (with length $T_n - T_p$) at each station and performed baseline correction and integration (single integration for velocity input time series, double integration for acceleration input time series) to obtain the displacement time series. We then applied an acausal Butterworth band-pass filter with corner frequencies at 0.01 and 15 Hz, and applied the Fourier transform to obtain the displacement spectrum of this signal.

[22] Finally, we invert the observed displacement spectra following the technique described in the previous section. We stopped the estimation process 20 seconds after the first P-wave detection. All time quantities discussed throughout the paper are referenced to the first P-wave arrival. That is, $t = 0$ corresponds to the P-wave arrival at the closest station.

[23] Possible sources of the scatter observed in the first few seconds of SI magnitude estimates (Figures 1b and 2b) include: unaccounted site amplification effects, mis-determination of the radiation pattern, and the fact that the estimates are based on a few seconds of P-wave data, with some stations having poor signal-to-noise ratio.

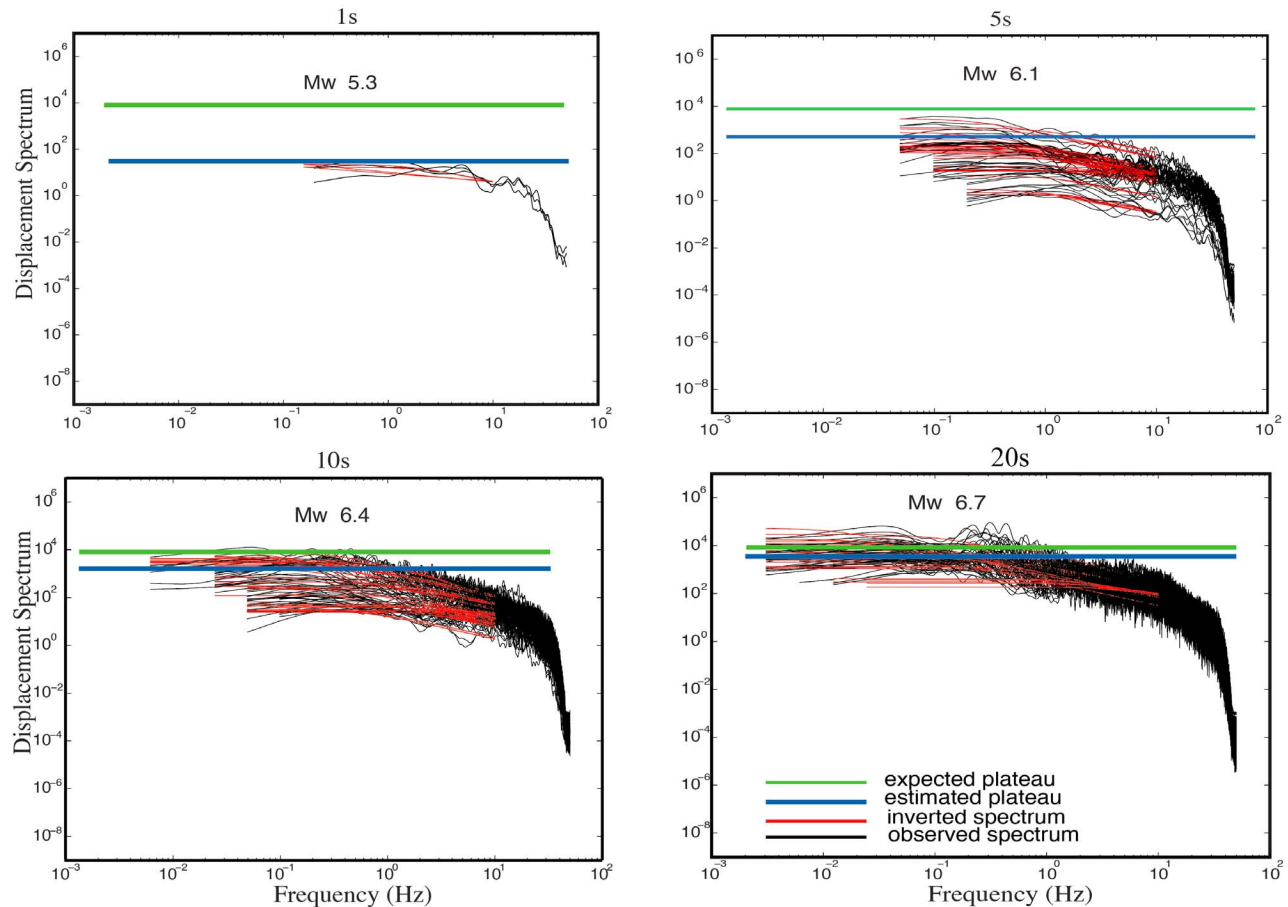


Figure 1b. The spectral inversion at 1, 5, 10 and 20 seconds from first P-arrival of the Mw6.9 Iwate-Miyagi earthquake. The observed spectra are shown in black, while the inverted plateau values are shown in red. The green line indicates the plateau level corresponding to the seismic moment calculated from the catalogue moment magnitude. The blue line indicates the average plateau level (from the seismic moment averaged across all contributing stations) at the given second.

3.2. Results

[24] Figure 2b shows the residuals between the SI magnitude estimate and the network magnitude as a function of time at various magnitude ranges for the combined dataset of Southern California and Japanese events. The histograms at 1, 5, 10, and 20 seconds after the first P-arrival at the network indicate the mean magnitude error and uncertainty of the SI magnitude estimates as a function of time. The mean error of the 1-sec SI magnitude estimates are consistently less than zero, indicating that the method systematically underestimates the network magnitude. This behavior is expected, since the estimate is based on a small portion of the P wave at a single station.

[25] At each site the lead time is defined as the difference between the S-wave arrival time, the time of the first P-phase detection at the network and the time needed to transmit and analyze the signal. The first warning can be issued when the first magnitude estimation is available, 2 sec in our method plus the telemetry delay. In this case the size of the blind zone (area with negative warning time) is smaller, and a larger lead time is available at the regions outside. However,

the location and magnitude estimates are affected by large uncertainties, and only some “low-cost” actions can be activated to protect the population. As time passes by, the magnitude estimate improves (we obtain stable values with smaller uncertainties), and a second warning can be raised. In this case the blind zone will be wider and the lead-time reduced, but a set of critical actions that required low level of uncertainties could be activated.

[26] There are 48 Southern California events in the $3 < M < 4$ magnitude range of our dataset. In this magnitude range, the 20-second SI magnitude estimates have an average over-estimation of 0.3 magnitude units. Possible reasons for this systematic overestimation include unaccounted site amplification effects and discrepancies between moment and local magnitude. Many of these events include stations located in the Los Angeles basin, where significant site amplification effects can be expected [Abercrombie, 1995]. Accounting for site amplification effects would potentially improve the convergence of the 20-second SI magnitude estimates to the network magnitudes.

[27] There are 14 Japanese events in the $6 < M < 7$ magnitude range of our dataset. Events in this magnitude

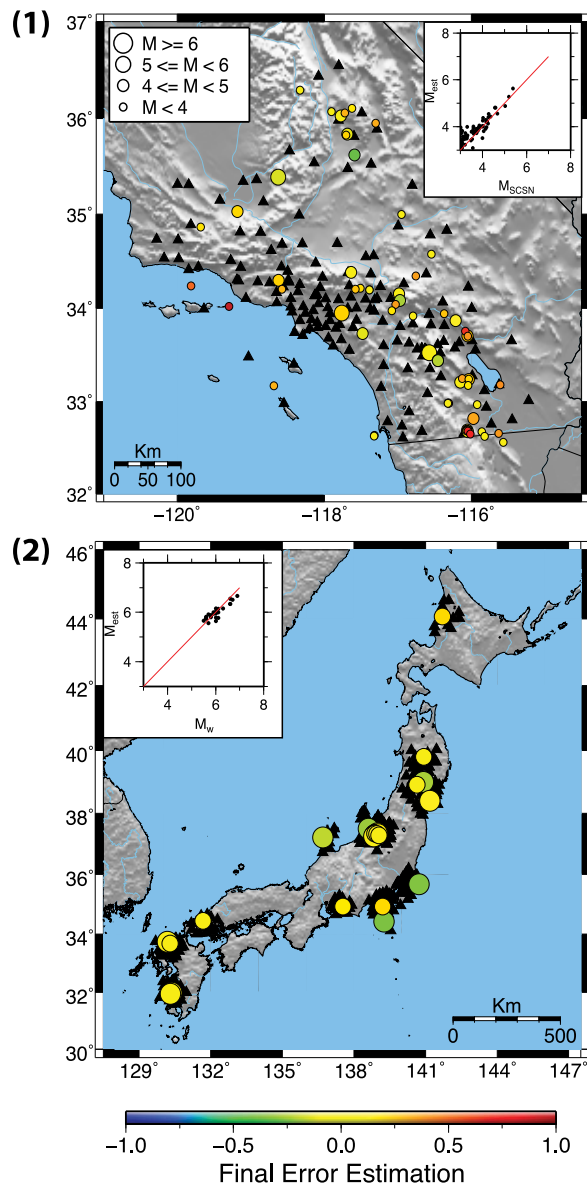


Figure 2a. Stations (black triangles) and events (colored circles) in (top) Southern California and (bottom) Japan used in our dataset. The color scale shows the SI magnitude error 20 seconds after the first P-wave detection. The inset plots show the 20-second SI magnitude estimate as a function of the network magnitude. The true regression line is shown in red.

range show a slower convergence towards the final magnitude. The spread of the 1 and 5 second histograms spans 2 orders of magnitude. There is evidence of convergence in the 20 second estimates, which exhibit a spread of less than 1 magnitude unit. The 20 second estimates have an average error of -0.3 magnitude units, indicating a systematic magnitude underestimation. This is related to our choice of stopping the estimation process 20 seconds after the initial P detection.

[28] Figure 2a shows that there is a strong spatial dependence (due to variations in station density) of the SI mag-

nitude errors in Southern California. In Southern California, most events in the interior of the network have 20-second magnitude errors close to zero. Errors are larger at the edges or outskirts of the network, such as south of the California-Mexico border, or off-shore along the Catalina islands. Such behavior is reasonable and cannot be avoided. It should be noted that the SCSN network solutions in these areas are also typically lower quality solutions, due to the lower station densities. There is less spatial heterogeneity in the final SI magnitude errors in Japan. The slight underestimation in the Japanese dataset is most likely due to limiting the estimation process to 20-seconds after the initial P-detection.

4. Conclusions and Discussion

[29] The Spectrum Inversion (SI) method is an evolutionary approach that operates on displacement spectra to estimate moment magnitude and its uncertainties. Assuming that the displacement spectra follows Brune's [1970] ω^{-2} model, this approach attempts to estimate the low frequency plateau of the displacement spectrum based on the portion of the spectra constrained by the available observations. Estimation can start as early as 1 second after the P-wave arrival at a single station, though a location estimate is necessary, and 1-second estimates consistently under-predict the network magnitude. We consider solutions "stable" once they are within (and stay within) 0.3 magnitude units of the network magnitude. Based on this criteria, we find that the SI magnitude estimation stabilizes within 10-seconds of the initial P-wave detection for both our Southern California and Japanese datasets.

[30] We tested this approach using broadband and strong motion waveforms recorded within 60 km of the source region for Southern California and Japanese events in the magnitude range $3.0 < M \leq 7$. Stable magnitude estimates are available within 10 seconds of the initial P detection for events with $M < 6$, with uncertainties decreasing as a function of time. The time for SI magnitude estimates to converge to the final catalogue magnitudes increases to 20 seconds (and possibly, larger) for stronger events. In fact, during the occurrence of a strong event, the algorithm operates while the rupture process is still ongoing; as consequence the Ω_0 initial estimates (and the related M_w values) underestimate the final magnitude. However such estimates can be interpreted as a minimum threshold for event size, giving the possibility to issue a first alert.

[31] SI and RTMag codes [Lancieri and Zollo, 2008] are both tested assuming that the location is given without uncertainties. In this case the convergence times are comparable on Kobe (M 6.9) and Noto-Hanto (M 6.7) events. For these events, the RTMag algorithm arrives at stable magnitude estimates within 12 seconds of the first P-phase detection. We can't compare with others "early warning" procedures as PRESTo, VS and Elarms, as they are complex softwares providing event detection, location, magnitude estimation and hazard evaluation.

[32] The main advantage of the SI method is its independence from locally-derived predictive or empirical relationships; it is based on a point source model and on the direct measures of physical quantities available at the network. The estimation time is comparable with other methods that operate on PGA, PGV, PD or predominant period. Due to its independence from predictive or empirical relationships, the

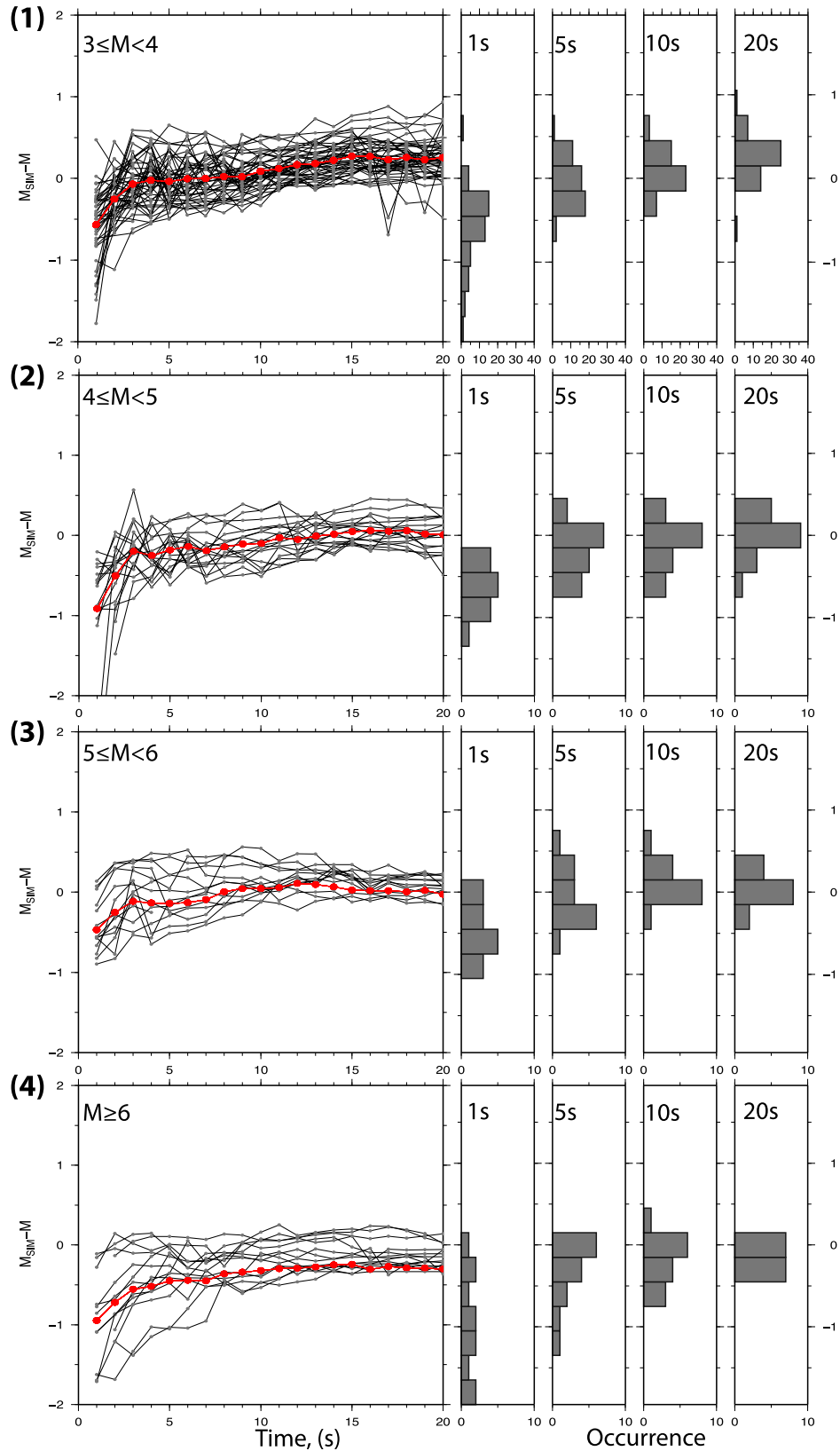


Figure 2b. The temporal evolution of SI magnitude error at various magnitude ranges, as well as histograms of SI magnitude error at 1-, 5-, 10- and 20-seconds. (top) We can see that the over-estimation for the smallest ($3 < M < 4$) and (bottom) the under-estimation for the largest ($6 < M < 7$) events in our database are always within an error of 1 magnitude unit after first 10 seconds, while (middle top and middle bottom) moderate events are quite well resolved after only 5–10 seconds.

SI method can be applied in any region without need for calibration of empirical relationships. In this study, we assumed the true location of the event, as listed in the earthquake catalogue. In this preliminary work we considered that the location is given without uncertainty. Future work will include applying the SI magnitude estimation approach in conjunction with an real time location algorithm [Horiuchi et al., 2005; Cua and Heaton, 2007; Satriano et al., 2008], and comparing its performance to other existing algorithms such as ElarmS, Virtual Seismologist, and PRESTo.

[33] **Acknowledgments.** We wish to thank the Associate Editor Ruth Harris and Kevin Mayeda and the anonymous reviewer for their comments and useful suggestions that helped us to revise and improve the manuscript. We also thank Matteo Spada and Claudio Satriano for their support and for useful discussion and comments. Strong motion and broadband waveforms for Southern California events were downloaded from the Southern California Earthquake Data Center (SCECDC) via Seismic Transfer Protocol (STP) (www.data.scecd.org/STP/stp.html), while the Japanese earthquake records was downloaded from the K-Net and KiK-net websites (www.k-net.bosai.go.jp).

References

- Abercrombie, R. (1995), Earthquake source scaling relationships from -1 to 5 ML using seismograms recorded at 2.5-km depth, *J. Geophys. Res.*, *100*(B12), 24,015–24,036.
- Aki, K., and P. Richards (2002), *Quantitative Seismology*, 2nd ed., Univ. Sci., Sausalito, Calif.
- Allen, R. M., and H. Kanamori (2003), The potential for earthquake early warning in Southern California, *Science*, *300*, 786–789, doi:10.1126/science.1080912.
- Allen, R. M., P. Gasparini, O. Kamigaichi, and M. Böse (2009), The status of earthquake early warning around the world: An introductory overview, *Seismol. Res. Lett.*, *80*(5), 682–693, doi:10.1785/gssrl.80.5.682.
- Allen, R. V. (1978), Automatic earthquake recognition and timing from single traces, *Bull. Seismol. Soc. Am.*, *68*(5), 1521–1532.
- Brune, J. N. (1970), Tectonic stress and the spectra of seismic shear waves from earthquakes, *J. Geophys. Res.*, *75*, 4997–5009.
- Cua, G. B., and T. Heaton (2007), The Virtual Seismologist (VS) method: A bayesian approach to Earthquake Early Warning, in *Earthquake Early Warning Systems*, edited by P. Gasparini, G. Manfredi, and J. Zschau, pp. 97–132, Springer, Berlin.
- Cua, G. B., M. Fischer, T. Heaton, and S. Wiemer (2009), Real-time performance of the Virtual Seismologist earthquake early warning algorithm in Southern California, *Seismol. Res. Lett.*, *80*(5), 740–747, doi:10.1785/gssrl.80.5.740.
- Espinosa-Aranda, J. M., A. Jiménez, O. Contreras, G. Ibarrola, and R. Ortega (2000), Mexico City Seismic Alert System, in *Proceedings of the International Symposium on Earthquake Disaster Prevention*, vol. 1, pp. 315–324, Cent. de Instrum. y Registro Sismico, Mexico City.
- Hanks, T. C., and H. Kanamori (1979), A moment magnitude scale, *J. Geophys. Res.*, *84*(B5), 2348–2350.
- Horiuchi, S., H. Negishi, K. Abe, A. Kamimura, and Y. Fujinawa (2005), An automatic processing system for broadcasting earthquake alarms, *Bull. Seismol. Soc. Am.*, *95*(2), 708, doi:10.1785/0120030133.
- Kamigaichi, O., et al. (2009), Earthquake early warning in Japan: Warning the general public and future prospects, *Seismol. Res. Lett.*, *80*(5), 717–726, doi:10.1785/gssrl.80.5.717.
- Lancieri, M., and A. Zollo (2008), A Bayesian approach to the real-time estimation of magnitude from the early P and S wave displacement peaks, *J. Geophys. Res.*, *113*, B12302, doi:10.1029/2007JB005386.
- Madariaga, R. (1976), Dynamics of an expanding circular fault, *Bull. Seismol. Soc. Am.*, *66*(3), 639–666.
- Satriano, C., A. Lomax, and A. Zollo (2008), Real-time evolutionary earthquake location for seismic early warning, *Bull. Seismol. Soc. Am.*, *98*(3), 1482–1494, doi:10.1785/0120060159.
- Satriano, C., L. Elia, C. Martino, M. Lancieri, A. Zollo, and G. Iannaccone (2010), PRESTo, the earthquake early warning system for Southern Italy: Concepts, capabilities and future perspectives, *Soil Dyn. Earthquake Eng.*, doi:10.1016/j.soildyn.2010.06.008, in press.
- M. Caprio, G. B. Cua, and S. Wiemer, Swiss Seismological Service, ETH Zurich, Sonneggstrasse 5, CH-8092 Zurich, Switzerland. (marta@sed.ethz.ch)
- M. Lancieri, École Normale Supérieure, 24 rue Lhomond, F-75230 Paris CEDEX 05, France.
- A. Zollo, Scienze Fisiche, Università Federico II di Napoli, I-80126 Napoli, Italy.